

Abstract

A ground penetrating radar (GPR) grid was collected to locate a Holocaust mass burial site in the Trakas-Pempiškis woods of Rokiškis, Lithuania. The survey, shot with a pulseEKKO Pro GPR system and 500 MHz antennae, consisted of 28 parallel GPR lines approximately 9 m in length and spaced 0.25 m apart. A Topcon RL-H4C laser leveler was used to measure topographic points surveyed every 1 sq. m. Historical eyewitness testimony and a truncation in subsurface stratigraphy beneath a surface depression suggested the presence of the burial site. Aiding interpretation of GPR data, we identified 13 unique Ordinary Kriging (OK) and Radial Basis Function (RBF) digital elevation models (DEMs) for GPR line topographic correction. Presumably, OK and RBFs produce DEMs passing through input points and predict values beyond minimum and maximum input point values, both desired attributes for logical consistency. In practice, OK and some RBF DEMs insignificantly exceeded minimum and maximum sample data values while other RBF DEMs exceeded both. Due to relatively large topographic sample point spacing, profiles are only adjusted for general trends in elevation change, and an analyst must be cognizant of individual lines' placement affecting uncertainty of correction.

Possible grid locations were determined by Jonas Rudokas' eye-witness testimony of the executions in the summer of 1941. Rudokas estimates around 28 executed Jewish Lithuanians were buried at the Trakas sites. Jewish **Kavod HaMet practices do not allow excavation of remains**, making GPR, a **non-invasive** subsurface imaging technique, an ideal investigatory tool (Jol and Bristow, 2003; Mieliauskienė et al., 2017). GPR data is collected by moving emitting and receiving antennae over the ground in small steps along lines. At each step radio frequency electromagnetic energy is emitted and wave reflections from the subsurface are recorded as a function of time.

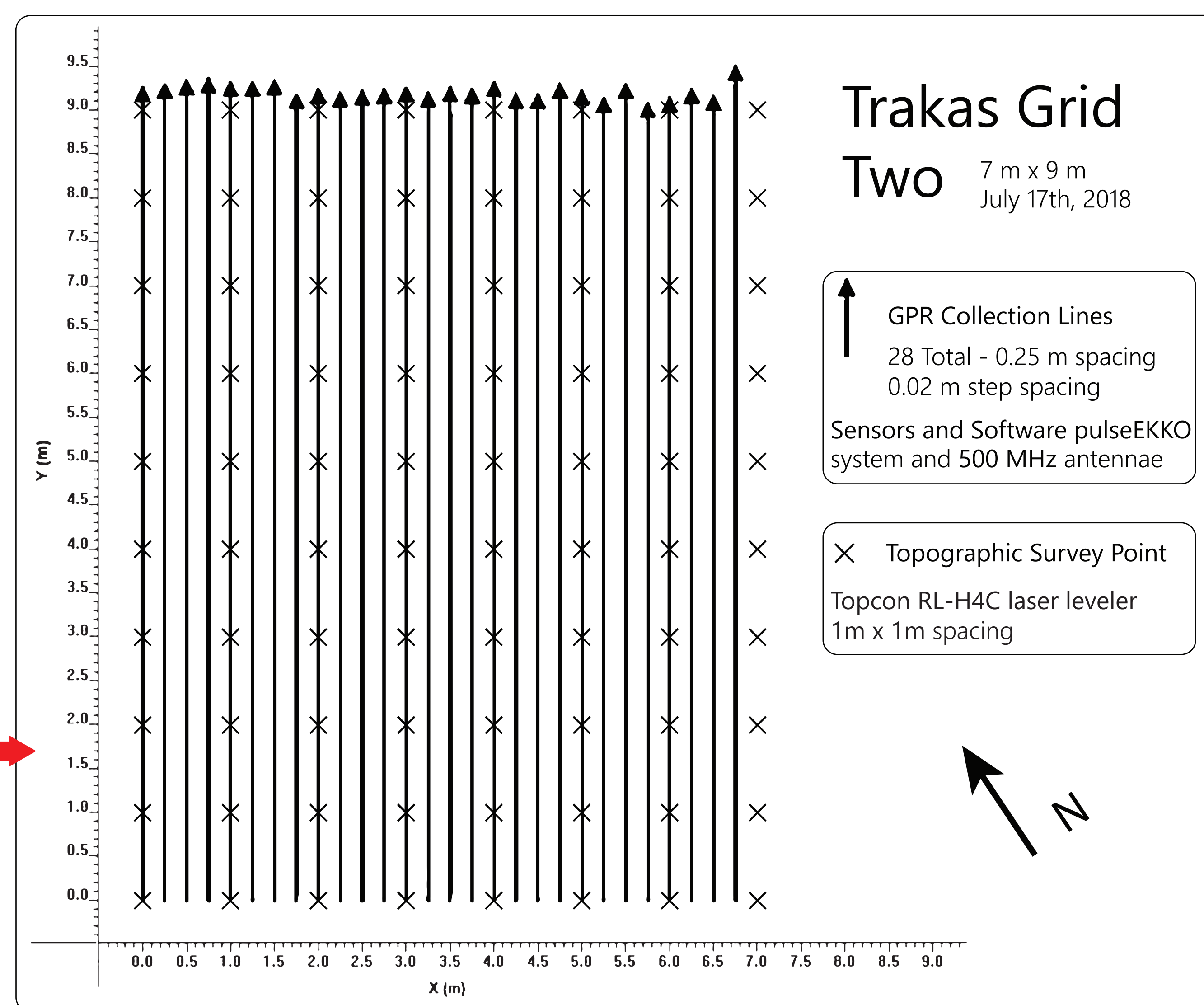


Local eye-witness identifying a burial site
Mieliauskienė et al. (2017)

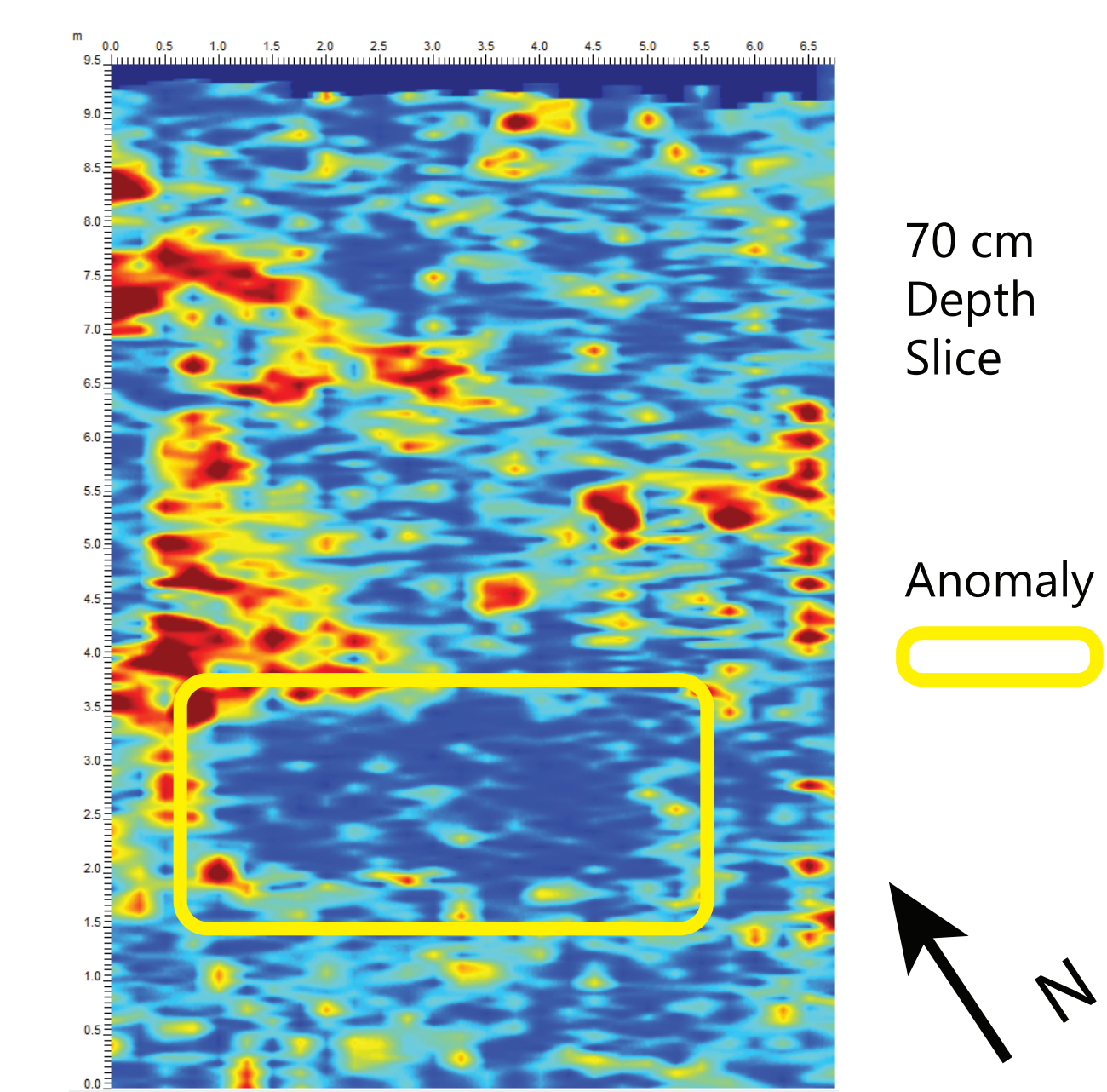


Grid two survey location in the Trakas-Pempiškis woods south of Rokiškis, Lithuania

Site Background



Transect specific data was post-processed and visualized as cross sectional profiles in Sensors and Software Ekko_Project Line View. Overall reflection strength was mapped for the entire grid in Slice View (below). An anomalous rectangular truncation in stratigraphy beneath a topographic depression, in conjunction with Rudokas' testimony, suggests the presence of the mass execution burial site (Fuerstenberg et al., 2018).

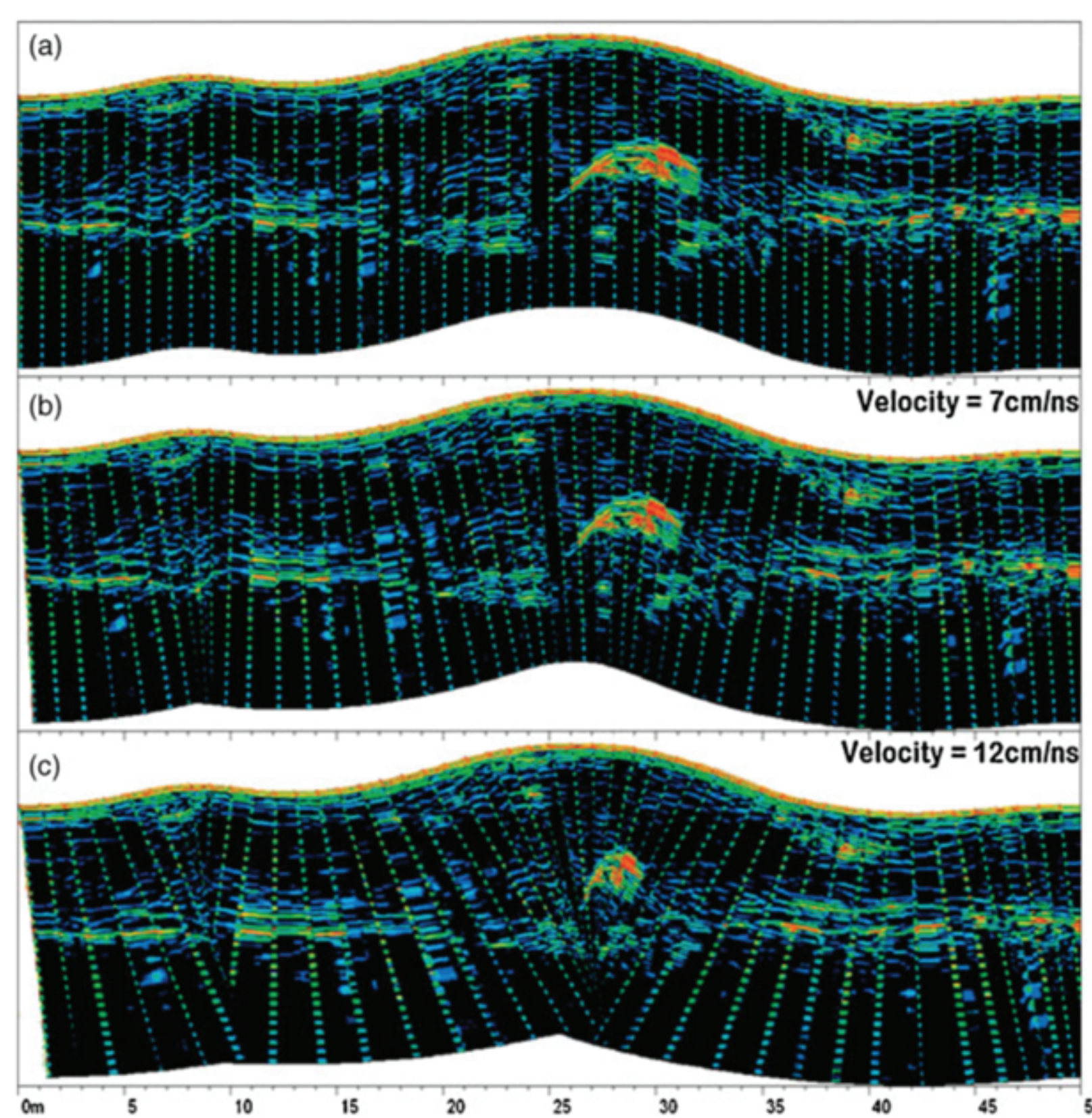


Goals

- Build and document clear and efficient workflows for GIS novices
- Build workflows in ESRI ArcMap, QGIS Desktop, and Golden Software Surfer for accessibility of methods in a variety of computing circumstances
- Execute and assess multiple interpolation algorithms for logical consistency
- Perform time-shift topographic correction with interpolated DEMs to aid interpretation of subsurface features

Methodological Background

Where **changes** in surface **topography** occur within a GPR line, topographic **correction** is needed for **accurate rendering** of subsurface features. Data from each step of a transect with minor surface relief can be simply **time shifted**, or vertically adjusted, to make meaningful geometric changes to subsurface features (Annan, 2008). Time shift correction can be performed natively in the Sensors and Software Ekko_Project software package.



Goodman, Nishimura, Hongo, and Higashi (2006)

- Profile (a) (above) has been **time shifted**.
- Profiles (b) and (c) have had trigonometric **tilt corrections** performed.
- Differences in stratigraphic reflection feature geometry between (b) and (c) reflect that with greater wave velocity, subsurface features are rendered deeper while the pulse paths extending perpendicular from the surface stay the same, resulting in horizontal stretching and shrinking of features. X-axis scales are not the same.

Topographic correction has been performed using DEMs such as those from terrestrial LiDAR, but there is currently no literature supporting use of DEMs interpolated from relatively **coarsely spaced laser leveling point data** (Zhang et al., 2014). Although both laser leveling and terrestrial LiDAR are precise surveying methods, laser leveling equipment is **cheaper** than terrestrial LiDAR scanning equipment and is **simpler** to obtain data from. Laser level surveying also does not require **overhead visibility**, making it an alternative to GPS for obscured areas like the forested Trakas site, and adding value to the development of laser level correction techniques in this study. Laser leveling surveys' downfall is **reliance on interpolation** to create a continuous DEM. Interpolation of low-survey data relative to the high-density data to be extracted from DEMs results in **underestimated slopes** and elevation **uncertainty** between observed points on the interpolated DEM (Aguilar et al., 2005; Chaplot et al., 2006).

Methods

1 Topographic Survey Data X, Y, Z

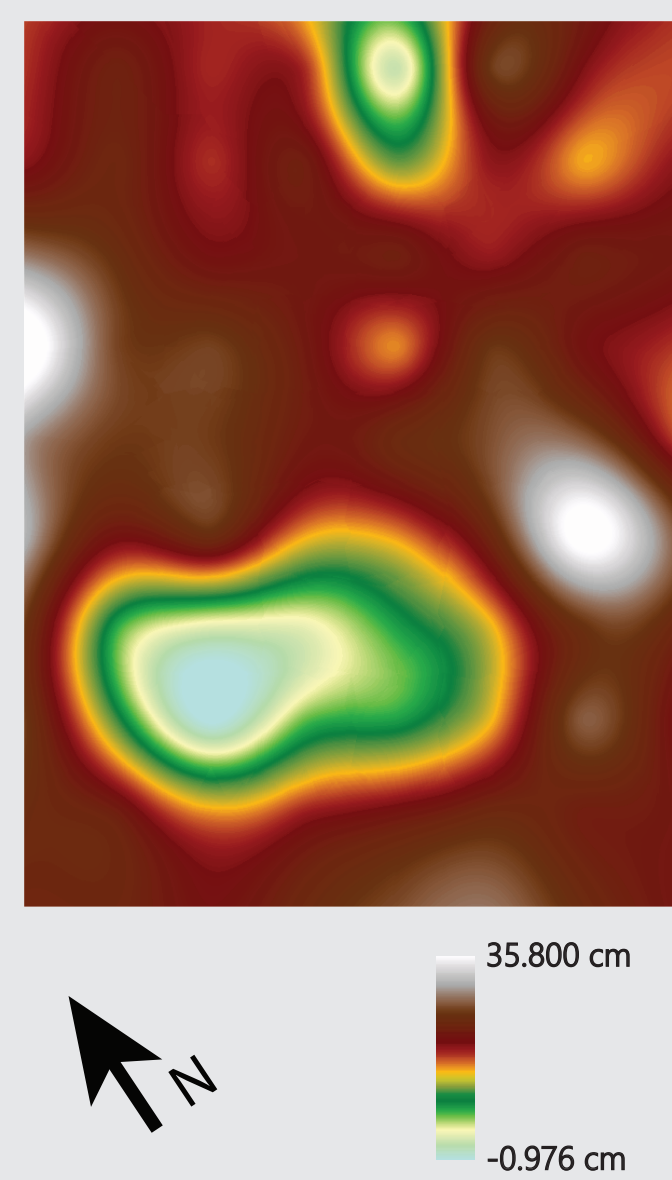
- Import into ESRI ArcMap and QGIS Desktop, create shapefile
- Interpolation can be performed simply with x, y, z data in Surfer

| Distance | Line | Elevation_m |
|----------|------|-------------|
| 0 | 0 | 0.218 |
| 1 | 0 | 0.23 |
| 2 | 0 | 0.242 |
| 3 | 0 | 0.24 |
| 4 | 0 | 0.292 |
| 5 | 0 | 0.281 |
| ... | ... | ... |

3 Raster DEM

- Resolution should be at or finer than step spacing

QGIS Desktop: Thin Plate Spline

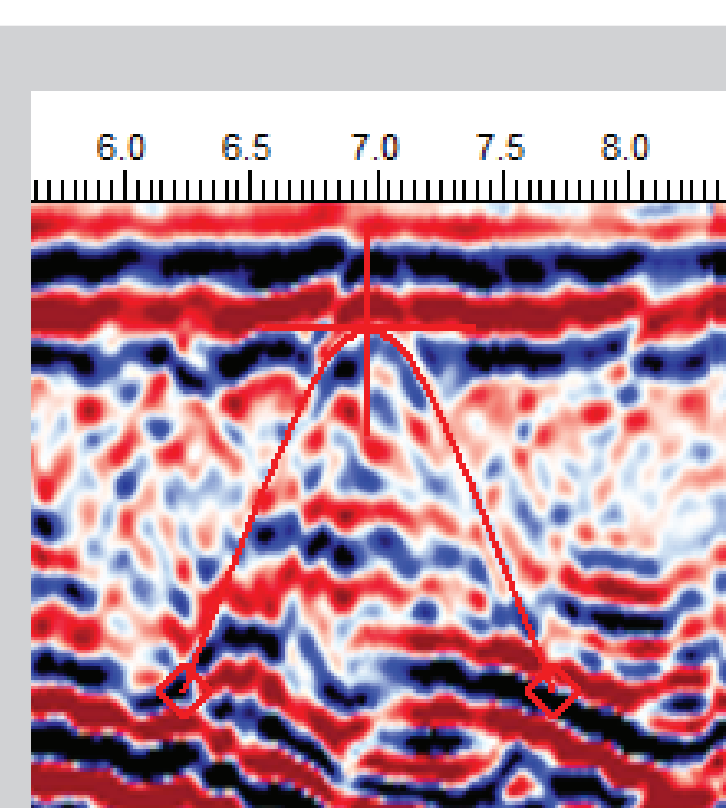


2 Perform Interpolation

- Extend output DEM Y axis to 9.5 m
- Use Ordinary Kriging (OK) and Radial Basis Function (RBF) techniques as they:
 - predict values beyond minimum and maximum input point values
 - produce DEM surfaces passing through the observed points
 - have been shown to produce the most accurate DEMs in experimental studies using similar point sampling schemes (Aguilar et al. 2005; Chaplot et al. 2006)
 - estimate values using values and distances of observed points in all directions, unlike line specific interpolations

4 Extract Points for Each Individual Line

- Use the "Extract Values by Table" tool in ESRI ArcMap
- Use the "Point sampling tool" plugin in QGIS Desktop
- Use "Point Sample" in Golden Software Surfer

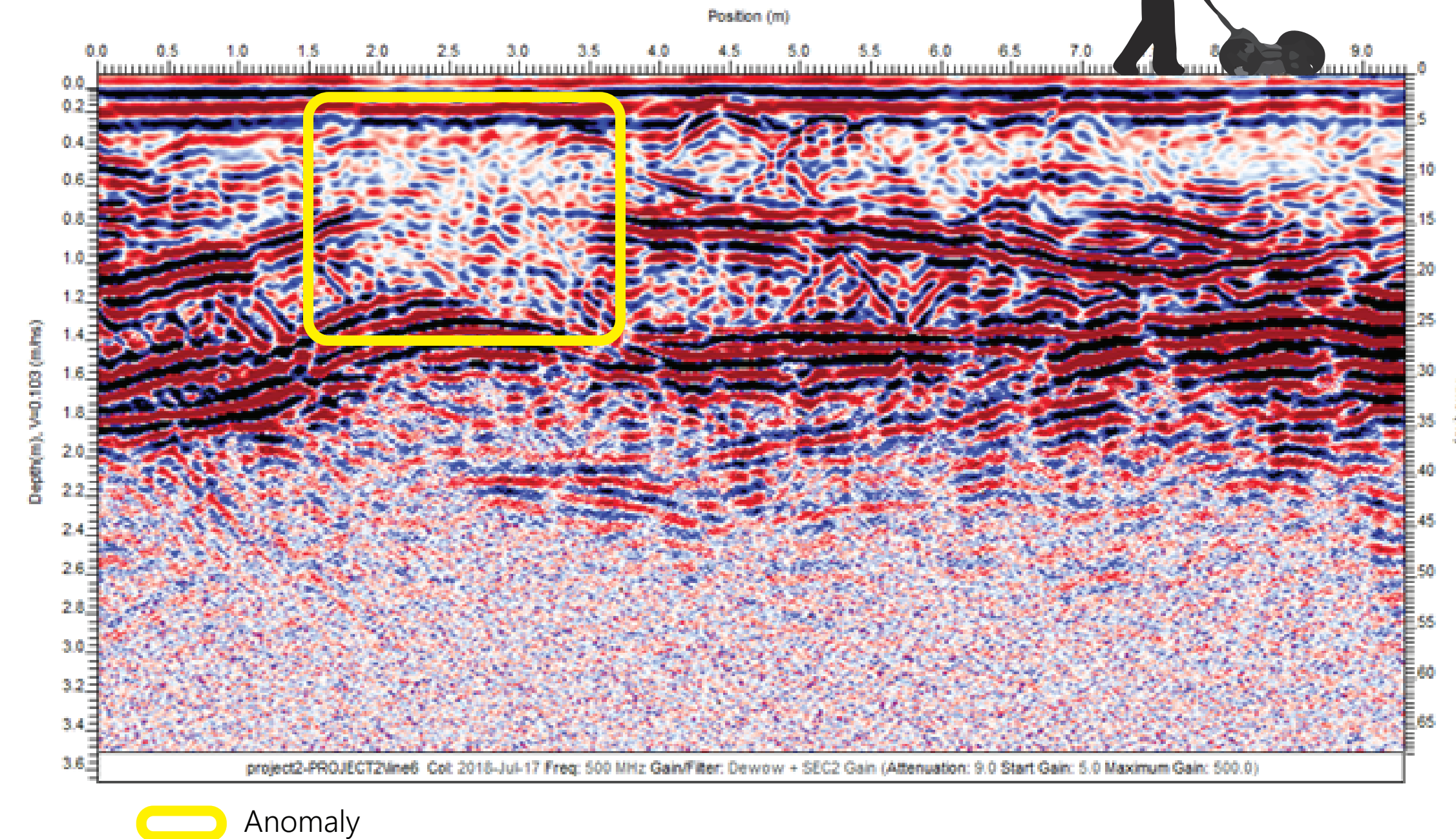


5 Topographically Correct GPR Data

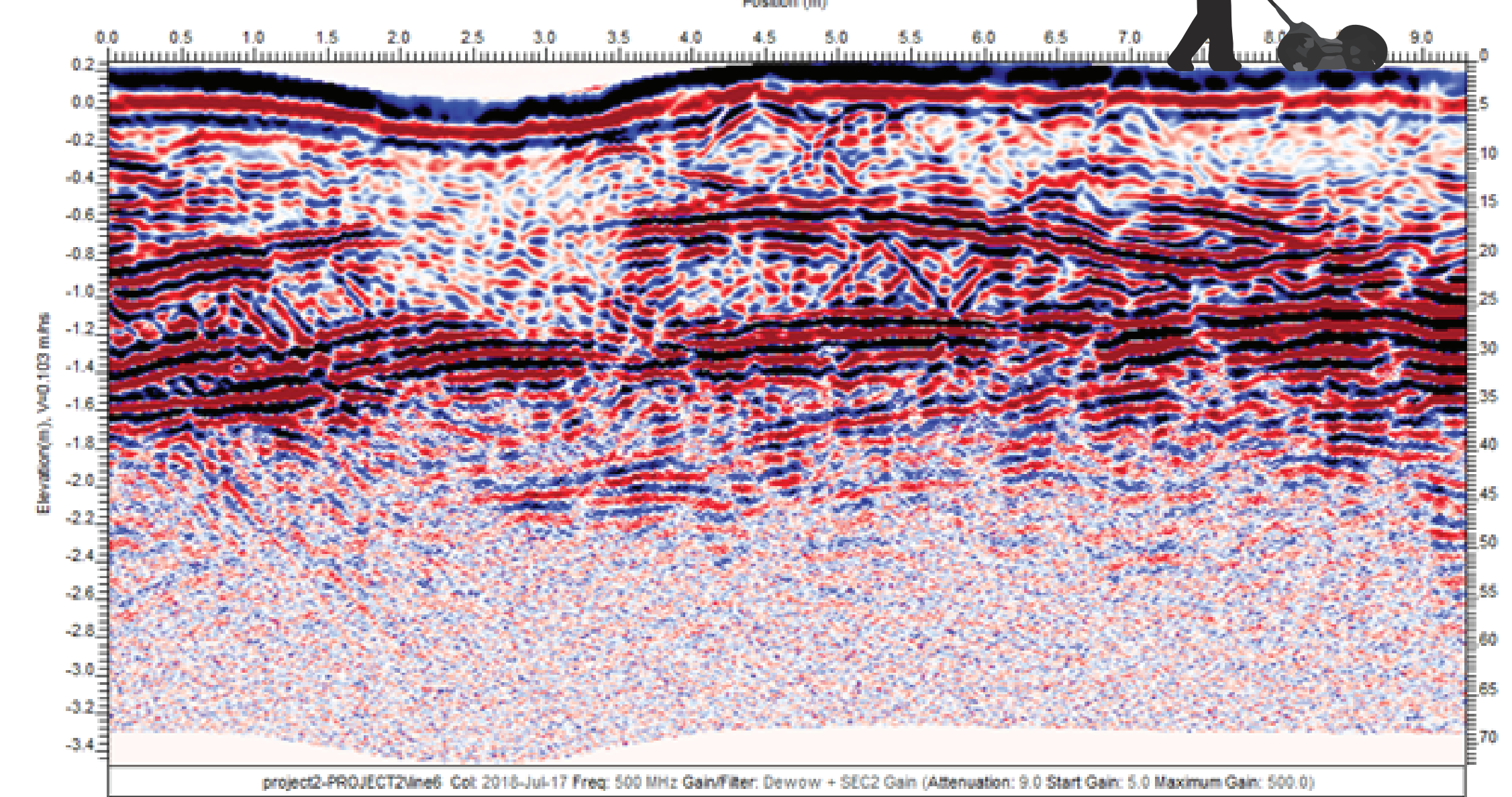
- Correctly format and bring line specific data into same folder as Sensors and Software Ekko_Project line files
- Open individual lines in Line View
- Use parabola matching (above, right) to find subsurface wave velocity
- Display Y-axis as depth instead of time

Results and Discussion

Line 6 Before time-shift correction



Line 6 After time-shift correction



Interpolated DEMs

- Peak and depression locations and elevations were estimated. Some interpolation methods did **not exaggerate** peak and depression elevation values or estimate alternative locations. Exaggerative methods only produced **minimal exaggerations** and location changes, suggesting non-exaggerating methods should **not be precluded** from use in correction in this instance.
- Differences between DEMs interpolated with the same method but in different software are due to parameters that were not able to be standardized within software interfaces.

Corrected GPR Profiles

- Because **uncertainty** in prediction **increases** with distance from observed points in interpolated DEMs, analysts must be cognizant of the **position** of any corrected line analyzed.
- A presumed **water table** in grid two's GPR transects is generally **flattened** after topographic corrections are performed, even on lines falling between observed points. If the flattened feature is the water table, flattening is an encouraging sign that interpolation methods tested somewhat **accurately predicted** elevations even along lines 0.5 m away from observed points (Annan, 2008).
- Interpolation methods performed could be used successfully at other **gridded sites** with **similar topographic** and survey **characteristics**. Guides were written to assist future researchers perform the methods developed in ESRI ArcMap, QGIS Desktop, and Golden Software Surfer.

Future Recommendations

- Three dimensional positions of **peaks** and **depressions** within the study grid may be **collected** to increase DEM accuracy.
- Time permitting, more **densely spaced** points may be collected over the entire grid to increase overall DEM accuracy. Alternatively, more points could be collected over specific areas of interest to increase those areas' accuracy.
- Provided clear overhead visibility, high accuracy integrated **GPS** and **inertial navigation system (INS)** data should be used instead of predicted elevations from interpolation. GPS and INS sensors provide **position** and **orientation** at each GPR shot. Because accurate orientation information is collected, **tilt-correction** can be performed resulting in **more accurate** geometric and positional **changes** to subsurface features (Conyers and Leckebusch, 2010; Goodman et al., 2006). Interpolated DEMs underestimates slope (Chaplot et al., 2006).

Acknowledgements

We would like to give thanks for the Student Budget Commitment Differential Tuition funds through the University of Wisconsin-Eau Claire Student/Faculty Research Collaboration Program and the Student/Differential Tuition through the University of Wisconsin-Eau Claire Student Travel for the Presentation of Research Results Program. We also would like to thank the Simpson Foundation for the Student Professional Travel Funding. We would like to acknowledge the Maurice Greenberg Center for Judaic Studies at the University of Hartford and the Rokiškis Regional Museum. We thank the University of Wisconsin-Eau Claire Learning and Technology Services for assistance in poster printing. Finally, we thank Dr. Harry Jol and Dr. Richard Freund for all of their support.

References

Aguilar, F. J., Aguilera, F., Aguilera, M. A., and Carvajal, E. 2005. Effects of terrain morphology, sampling density, and interpolation methods on grid DEM accuracy: Photogrammetric Engineering and Remote Sensing, v. 71, no. 7, p. 805-816.
 Annan, A. P. 2008. Electromagnetic Principles of Ground Penetrating Radar. In Jol, H. M., ed., Ground Penetrating Radar: Theory and Applications. Amsterdam, Elsevier Science, p. 4-40.
 Chaplot, V., Darboux, F., Bouroumane, H., Leguédic, S., Silveira, N., and Phachomphon, K. 2006. Accuracy of interpolation techniques for the derivation of digital elevation models in relation to landform types and data density: Geomorphology, v. 77, no. 1-2, p. 126-141.
 Conyers, L. B., and Leckebusch, J. 2010. Geophysical Archaeology Research Agendas for the Future: Some Ground-penetrating Radar Examples. Archaeological Prospection, v. 17, no. 2, p. 117-123.
 Fuerstenberg, M. M., Jol, H. M., Freund, R. A., Jaročnick, R., Kujelis, G., Reeder, P. P., Beck, J. D., Kolman, C. C., Schneider, S. G., 2018. Ground penetrating radar imaging of the Trakas Holocaust Mass Grave, Lithuania: Geologic Society of America Abstracts with Programs, v. 50, no. 6.
 Goodman, D., Nishimura, Y., Hongo, H., and Higashi, N. 2006. Correcting for topography and the tilt of ground-penetrating radar antennae. Archaeological Prospection, v. 13, no. 2, p. 157-161.
 Jol, H. M., and Bristow, C. S. 2003. GPR in sediments: Advice on data collection, basic processing and interpretation, a good practice guide: Ground Penetrating Radar in Sediments: Geological Society, London, Special Publications, v. 211, p. 9-27.
 Mieliauskienė, M., Kujelis, G., and Rudokas, J. 2017. Identification of a Holocaust Site in the Trakas-Pempiškis Woods in the Kamajai Eldership of the Rokiškis Region: Rokiškis Regional Museum press release.
 Zhang, D., Zhong, R. F., Li, J. C., and Zeng, F. Y. 2014. Topographic correction of GPR profiles based on laser data. In Proceedings 35th International Symposium on Remote Sensing of Environment (ISRSE35), Institute of Remote Sensing & Digital Earth, Beijing, People's Republic of China, Apr. 22-26, 2013, Volume 17: Bristol, Top Publishing Ltd.

| Surfer | Min (cm) | Max (cm) |
|-------------------------------|------------|----------|
| Thin Plate Spline | -1.356 | 35.803 |
| Ordinary Kriging | -1.550e-11 | 35.800* |
| Multiquadratic | -0.772 | 35.800* |
| Multilogarithmic | -0.232 | 35.801 |
| Natural Cubic Spline | -1.697 | 35.815 |
| ArcMap | Min (cm) | Max (cm) |
| Thin Plate Spline | -0.838 | 35.800* |
| Ordinary Kriging | -1.651e-17 | 35.800* |
| Multiquadratic | -1.416 | 35.803 |
| Inverse Multiquadratic | -1.561 | 35.806 |
| Completely Regularized Spline | -1.416 | 35.803 |
| Spline with Tension | -0.778 | 35.800* |
| QGIS Desktop | Min (cm) | Max (cm) |
| Thin Plate Spline | -0.976 | 35.800* |
| Multi-level B-spline | -0.188 | 35.932 |

Bold: method was executed in multiple software packages
* Did not exceed extent of input dataset